

**FACULTY
OF MATHEMATICS
AND PHYSICS**
Charles University

BACHELOR THESIS

Martin Vaněk

**Optimization of the Performance
of Fuel Cell Stacks
Using an Ultrasonic Humidifier.**

Department of Surface and Plasma Science

Supervisor of the bachelor thesis: Mgr. Yurii Yakovlev, Ph.D.

Study programme: Physics

Study branch: FP

Prague 2022

I declare that I carried out this bachelor thesis independently, and only with the cited sources, literature and other professional sources. It has not been used to obtain another or the same degree.

I understand that my work relates to the rights and obligations under the Act No. 121/2000 Sb., the Copyright Act, as amended, in particular the fact that the Charles University has the right to conclude a license agreement on the use of this work as a school work pursuant to Section 60 subsection 1 of the Copyright Act.

In date

Author's signature

I would like to thank my supervisor, Mgr. Yurii Yakovlev, Ph.D., for all his time, help and patience with this work.

Also a huge thank you belongs to my family, girlfriend, and friends for their support with my studies and all the other endeavors.

Title: Optimization of the Performance of Fuel Cell Stacks Using an Ultrasonic Humidifier.

Author: Martin Vaněk

Department: Department of Surface and Plasma Science

Supervisor: Mgr. Yurii Yakovlev, Ph.D., Department of Surface and Plasma Science

Abstract: This work is concerned with the optimization of the performance of PEM hydrogen fuel cell stacks, a technology that opens up new possibilities for clean energy storage and restoration. We have hand-built a PEMFC open-cathode stack of 20 cells and measured its basic characteristics such as the j-V and j-P curves as well as the dependency of the temperature of the stack on power produced by the stack for constant power of the cooling fans. We have implemented and tested the performance of a new method for water and thermal management – the humidification of air via the use of an ultrasonic water fog generator. Several tests – measuring cooling efficiency, voltage variations between different cells, and j-V and j-P curves – were performed under different temperatures and with or without humidification.

Keywords: fuel cell, self humidification, open cathode, performance

Název práce: Optimalizace svazků palivových článků pomocí ultrazvukového zvlhčovače.

Autor: Martin Vaněk

Katedra: Katedra fyziky povrchů a plazmatu

Vedoucí bakalářské práce: Mgr. Yurii Yakovlev, Ph.D., Katedra fyziky povrchů a plazmatu

Abstrakt: Tato práce se zabývá optimalizací výkonu svazků PEM palivových článků, technologie, která otevírá nové možnosti pro uskladnění a zpětnou výrobu elektrické energie. Sestavili jsme dvaceticelový sériový svazek PEM vodíkových palivových článků s otevřenou katodou a změřili jeho základní charakteristiky, jako jsou j-V a j-P křivky a také závislost teploty článku na výkonu, který produkuje za konstantního výkonu chladících větráků. Implementovali a otestovali jsme novou metodu pro správu vody a teploty článku – zvlhčování příchozího vzduchu pomocí ultrazvukového generátoru mlhy – a její vliv na výkon svazku. Provedli jsme několik testů – měření efektivity chlazení, variací v napětích na jednotlivých celcích a j-V a j-P křivky – a to za různých podmínek, konkrétně při různých teplotách a se zvlhčováním či bez něj.

Klíčová slova: palivový článek, samozvlhčování, otevřená katoda, výkon

Contents

Introduction	2
1 Theoretical Foundations	3
1.1 The Fuel Cell	3
1.1.1 PEMFC	3
1.1.2 Structure	3
1.2 Basic Characteristics of a Fuel Cell	5
1.3 Fuel Cell Stacks	6
1.3.1 Water and Thermal Management	8
1.4 Power Lost by the Stack	9
2 Measurement	10
2.1 Equipment	10
2.2 Building the Stack	10
2.3 Measurement Error	11
2.3.1 Uncertainty in Temperature	12
2.3.2 Unusable Measurements	15
2.3.3 Other Sources of Error and the Total Error	15
2.4 Basic Characteristics	16
2.5 Artificial Humidification via Piezoelement	17
2.6 Measuring the Efficiency of Cooling	18
2.6.1 Voltage Deviations	21
2.7 Comparison – With and Without Humidification	25
2.8 Thermal Maps of the Stack	26
3 Discussion of the Results	27
3.1 Basic Characteristics	27
3.2 Voltage Deviations	27
3.3 Systematic and Statistical Error	27
3.4 Power Lost to Heat and Cooling	27
3.5 The Effects of Humidification	28
3.5.1 Additional Weight Added by Humidification System	29
3.6 The Disregarded Measurements	29
3.6.1 The 45 °C Humidification Measurement	31
Conclusion	32
Bibliography	33
List of Figures	36
List of Abbreviations	37

Introduction

Despite the ever-growing energy demands and the lurking climate crisis, most of the world's electricity is still being produced by burning fossil fuels, and in 2020, only 16 % of energy came from low-carbon sources.[1] This fact is further alarming considering that air pollution caused by burning fossil fuels is responsible for a full fifth of all the premature deaths worldwide (8.7 million in 2018 alone [2]).

In the need of clean energy sources and management, none of the available technologies can plausibly solve the crisis by itself. Several technologies are likely to play an important role in the energy revolution, e.g. nuclear fission, fusion, hydro, and, perhaps most notably, solar and wind energy. The last two are already being widely used but suffering from large variance in power output caused by the weather and/or daytime, geographical location etc. [3].

Thus, there is a need for energy storage to meet the actual demands. One option is using batteries and super capacitors that can store the electricity “directly”. Another option is obtaining hydrogen (e.g. via electrolysis) and storing it as an intermediate on the way of electricity production via the use in hydrogen fuel cells. Though hydrogen cycle has some drawbacks, such as lower overall energy conversion efficiency, problem with storage, or safety issues, the use of hydrogen has crucial advantages over batteries, such as fast refilling/recharging, or up to sixty times larger specific energy density (in $\text{J} \cdot \text{kg}^{-1}$) [4].

One of the most promising types of fuel cells are PEMFCs (proton-exchange membrane fuel cells) that are special among other types of fuel cell due to their ability of operation at low temperatures and in a variety of appliances including automotive and airborne [5].

To achieve a sufficient power output for practical applications, fuel cells are assembled into stacks, which are then further embedded in larger systems enabling proper fuel and temperature management for optimal function.

For lower power requirements, and where lighter weight is critical, such as in drones, much of the balance of plant of the stack can be omitted by using an open-cathode stack, where the supplied air is used both as a source of oxygen and a coolant. To increase the air (and therefore oxygen and coolant) inflow, the air can be pushed into the stack, e.g. using a ventilator fan (forced convection) [see e.g. 6].

Despite (or more precisely, because of) this greatly simplified design, open-cathode stacks have the disadvantage of being highly dependent on the ambient conditions, such as air humidity or temperature. Thus, proper management of those conditions and the stack's response to them is of crucial importance for achieving high performance.

This work is concerned with open-cathode forced convection stacks of PEM hydrogen fuel cells, in particular, the methods for optimizing and measuring their power output. We present and test out a new way of water and thermal management via humidification of the incoming air with an ultrasonic water fog generator.

1. Theoretical Foundations

1.1 The Fuel Cell

The fuel cell provides a way of creating electrical energy from stored chemical energy in hydrogen (and other fuels).

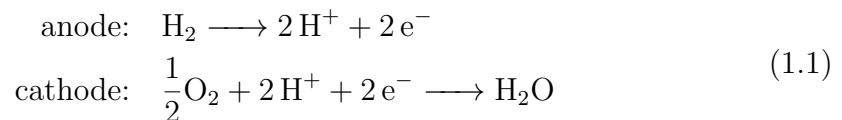
There are many types of fuel cells that can be powered by hydrogen, most notably differentiated by the material of their membrane electrolyte assemblies and the chemical reactions taking place inside them, such as [7]

- phosphoric acid fuel cell (PAFC),
- polymer electrolyte membrane fuel cell (PEMFC),
- alkaline fuel cell (AFC),
- molten carbonate fuel cell (MCFC), or
- solid-oxide fuel cell (SOFC).

We will concern ourselves with PEMFC, which is considered to be the most promising type of fuel cell for portable applications due to its low-temperature operation, fast start-up, and versatility.[5]

1.1.1 PEMFC

The basis of PEMFC is a polymer membrane that is conductive to protons (i.e. ionized hydrogen). The reactions on the electrodes are [7]



The membrane is very thin (20–200 μm) and flexible and needs to be hydrated by water for proper conductive properties. Thus, water management is of crucial import. One of its consequences is a limit on the operating temperatures of the stack (typically below 80 °C).[7] This low temperature implies the usage of extremely active catalysts, such as the very expensive Platinum, for optimal performance.

The advantages of PEMFC include the highest power density of all the fuel cells, good start-up/shut-down capabilities and low operating temperature.

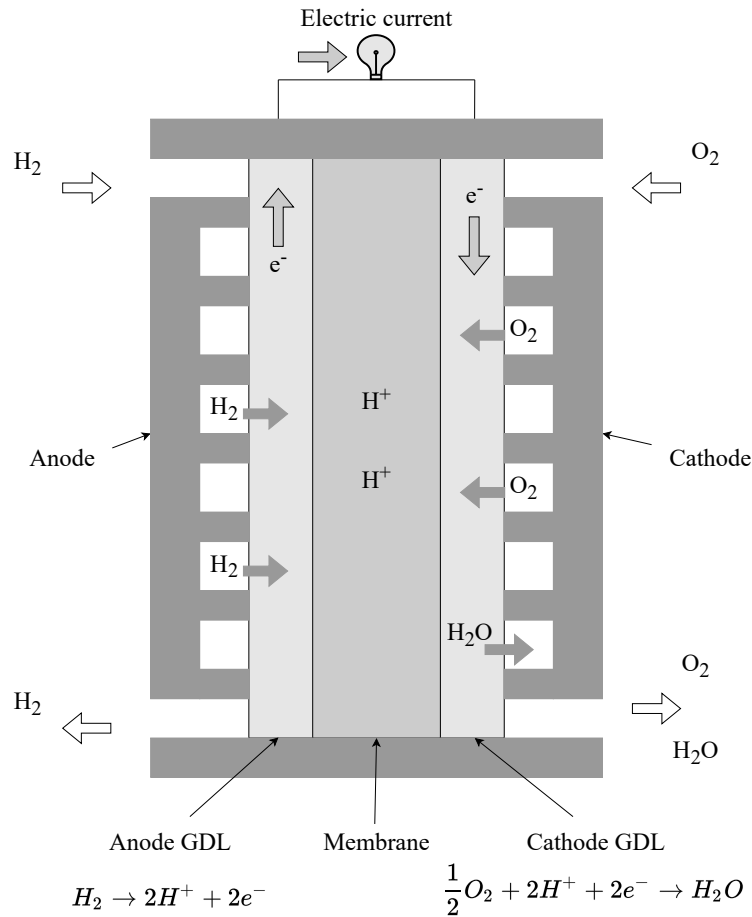
Among its disadvantages, we may find the aforementioned cost or complex water and thermal management.[5]

1.1.2 Structure

The active part of the PEMFC consists of several layers creating an almost symmetrical sandwich-like structure, as shown in fig. 1.1. The middle part is the polymer electrolyte membrane itself. Then, symmetrically, catalytic layer (in our

case Platinum-based) and GDL – gas diffusion layer.¹ All of these inner parts of a fuel cell are also called MEA – membrane electrolyte assembly. Outside the MEA, there are two bipolar plates – a cathode and an anode.

Figure 1.1: Schema of a PEMFC fuel cell.



For the oxidant gas, pure oxygen is often used in laboratory conditions for precise measurements. However, for portable applications, the oxygen comes with additional weight and storage capacity needed, which makes its usage impractical. Therefore, using ambient air as an oxidant is often preferred.[5]

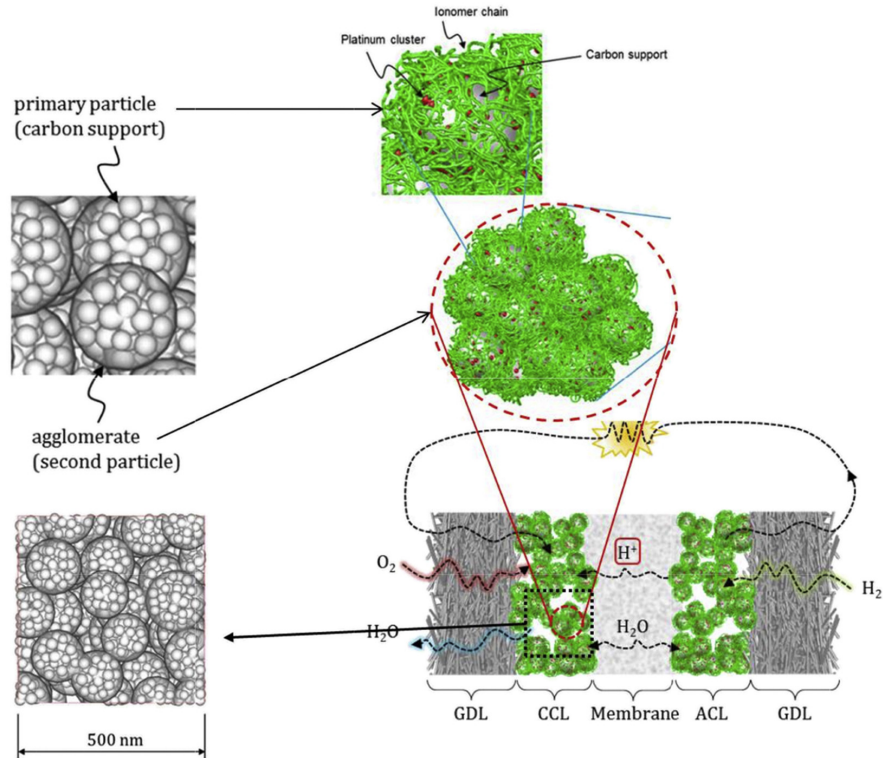
The catalytic layer itself is rather complex. It is a porous structure which consists of ionomer phase (for PEMFC a proton conductive material) mixed with catalyst nanoparticles (usually carbon-supported).

The performance of the fuel cell and the water management are highly dependent on the micro-structure of the catalytic layer, GDL pore size, the microporous layer etc.[8, 9, 10, 11, 12, 13]

The micro-structure of the catalytic layer is shown in fig. 1.2.

¹The catalyst can be attached either on the membrane, or on the GDL. If it is on the GDL, then GDL+catalyst are referred to as GDE – gas diffusion electrode.

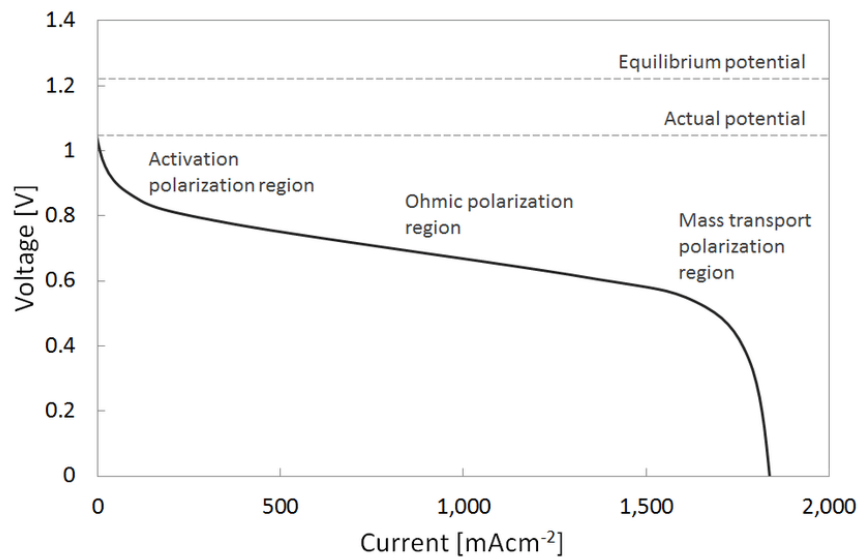
Figure 1.2: Micro-structure modeling of the agglomerate catalyst layer [from 14].



1.2 Basic Characteristics of a Fuel Cell

One of the most fundamental characteristics of a fuel cell is its polarization curve, i.e. the dependency of voltage on current (or, more commonly, current density). A typical polarization curve for PEMFC is shown in fig. 1.3.

Figure 1.3: A typical polarization curve of a PEM fuel cell [taken from 15].



We can divide the curve into 3 parts: in the first one, there is an exponential voltage decay caused by activation potential needed for the electrochemical reaction. The second part of the characteristic is linear (“ohmic region”) where the ohmic resistance associated with the transport of ions and electrons through the

cell is dominating. The last part sees a rapid decline in voltage once again due to mass transfer limitations of the electrode [16].

1.3 Fuel Cell Stacks

Since single cells are thermodynamically limited in their voltages (and in practice typically in the range of 0.6 – 0.8 V), they are usually assembled into stacks to achieve the desired power output and convenient voltage for larger applications (drones, cars etc.).

Although the functioning of single cells and that of stacks differ somewhat, it has been shown that many of the basic characteristics for stacks are simply additions of the values on individual cells (see e.g. [17]).

A stack consists of several MEAs separated by bipolar plates (that serve as a cathode on one side and an anode on the other). The outermost parts of the stack are the end plates (that serve only as one electrode each). The cells inside the stack have a common hydrogen supply. The stack is usually compressed at high pressure and then sealed by bolts to prevent any leakage of fuel that would render the stack unusable.

For a complete and functioning system, several components, such as a hydrogen storage, humidifier, or a device for air flow control, are needed apart from the stack itself. Some of them are associated with parasitic load that needs to be taken into account for assessing the performance of the stack in practice, see e.g. [18]. There are several ways of assembling these systems. Two of them are shown in fig. 1.4.

In the “typical” or closed cathode system, the inward airflow is controlled via a compressor (and a cooler), as shown in part a) of the fig. 1.4 whereas in an “open-cathode” system, which is the focus of this work, much of the structure is omitted and replaced by a simple fan². This has the advantage of greatly simplifying the system and lowering its weight, however, it also means that the power output is much more dependent on the surrounding conditions since the properties of the incoming air, such as temperature or humidity, on which the performance of the stack highly depends [19], are not controlled.

The airflow is also harder to control in the open-cathode systems meaning that heat management or the amount of reactant may be inadequate for the system. Thus, a proper water and thermal management is crucial for open-cathode systems.³

A schema of an open-cathode stack is shown in fig. 1.5.

²Which is itself sometimes omitted in so-called “free-breathing” systems. However, we will not concern ourselves with these.

³The hydrogen supply is common to all cells even in the open-cathode stack and is much easier to control.

Figure 1.4: Designs of PEMFC systems: (a) typical and (b) open cathode system [taken from 5].

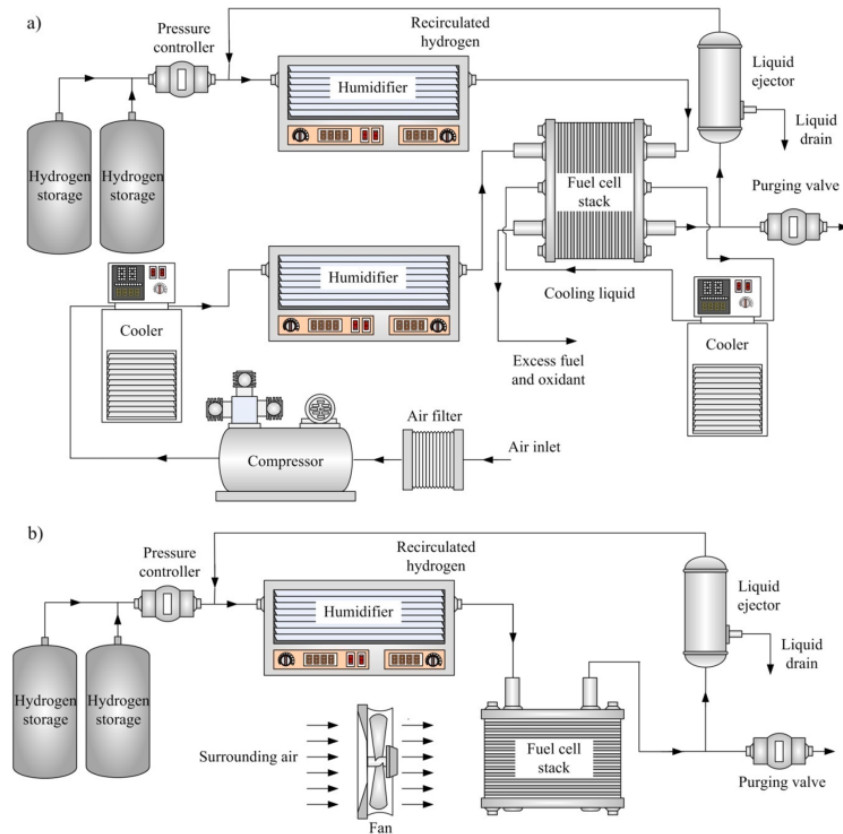
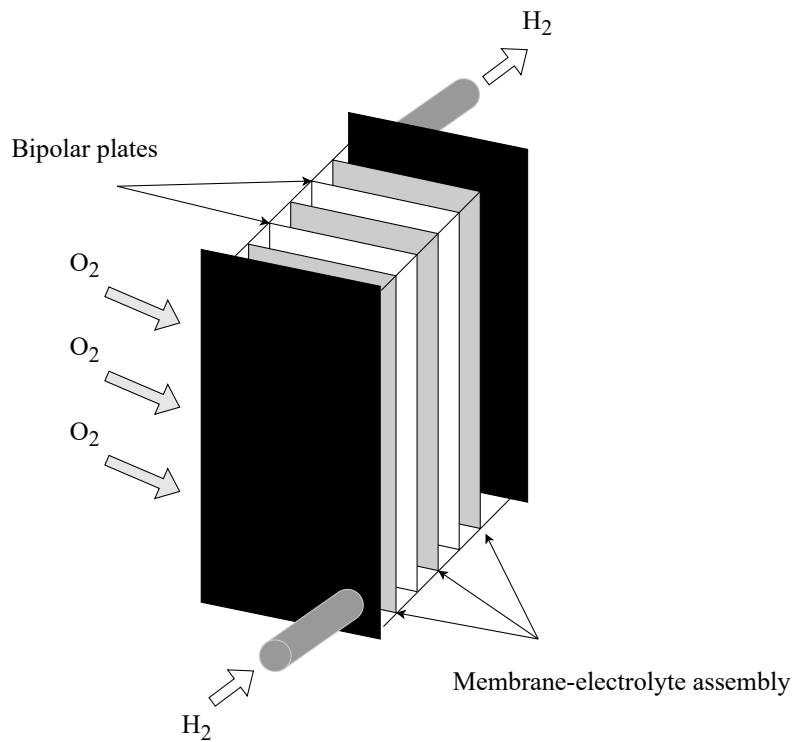


Figure 1.5: Schema of an open-cathode stack.



1.3.1 Water and Thermal Management

As mentioned previously, the PEM needs to be properly hydrated for optimal functioning. Thus, once the membrane is hydrated, the rate of water removal and generation should be equal, making the problem of water management crucial.

There are two problems with water management that can lead to poor performance – flooding (when there is too much water in the stack that blocks the catalyst pores and can also corrode the carbon of PEMFC [20]) and dry-out (when there is too little water).

As can be seen from the equation (1.1), water is created at the cathode side of the cell itself, thus, it can be recycled and used for humidifying the stack (so-called *self-humidification* regime). In an ideal case, the water produced by the stack would be sufficient by itself, however, in reality, some of the water will inevitably evaporate, creating the need for further humidification. Luckily, it is sufficient to humidify the cathode side, as the water can flow through the membrane to the anode side.

To prevent water from flooding the anode side of the membrane, it needs to be disposed of. In laboratory conditions, this is achieved by increasing the stoichiometry of hydrogen that drives out the water. In practice, however, this is too wasteful, thus, so-called dead-end mode is used. In the dead-end mode, there is hydrogen inflow to the anode, but the outflow valve is closed most of the time, and only opened periodically to remove the waste reactants that would otherwise clog the cell.

As noted before, the temperature of the stack is limited to prevent too much water from evaporating and causing dry-out. However, higher temperatures are desirable as the ionic conductivity of the membrane increases with temperature. So, although functioning PEMFC were demonstrated even at temperatures around 120 °C (see [21]), the optimal temperature for PEMFC stacks tends to be lower.

As thermal management is of crucial import, many attempts have been made to model and otherwise improve it, e.g. via implementing new technologies – [22] tried integrating an ultra-thin vapor chamber – or by investigating the optimal values of parameters such as fuel cell length, cathode channel height etc. [23].

In the open-cathode, forced-convection stacks, the amount and speed of the incoming air can be regulated by a ventilator fan. This air then serves several purposes, among them are oxygen supplying and cooling the stack. This combined dependency poses several problems, making the water and thermal management more difficult. For example, for a given power output, the stack may produce too much heat, thus, more fan power is needed to cool it down and prevent dry-out. However, the additional airflow can bring too much reactant, causing flooding and impairing the performance.

1.4 Power Lost by the Stack

Not all the power produced by the stack can be converted to electrical energy, inevitably, losses are incurred and waste heat is produced. The power “lost” by the stack⁴ is

$$P_{loss} = In(U_{max} - U), \quad (1.2)$$

where I is the current going through the cell, n is the number of cells, U is the actual average voltage of the stack cells, and $U_{max} \approx 1.48$ V is the thermoneutral potential, which is defined as $h/(NF)$, where $h \approx 286$ kJ · mol⁻¹ is the molar enthalpy of “H₂ + O₂ → H₂O” reaction, $N = 2$ is the number of electrons in the reaction, and $F \approx 96.5$ kC · mol⁻¹ is the Faraday constant [24].

By analyzing the dependency of this power lost on the duty cycle of the cooling fans⁵, we obtain the measure of the efficiency of cooling, which shows the potential for practical usage. For example automatized controlling units can use this characteristic to function much more efficiently and precisely. Another use of these data is in modeling the internal workings of the stack.

⁴Note that this is simply the difference between the “maximal theoretical” voltage that the stack could thermodynamically produce and the actual measured voltage.

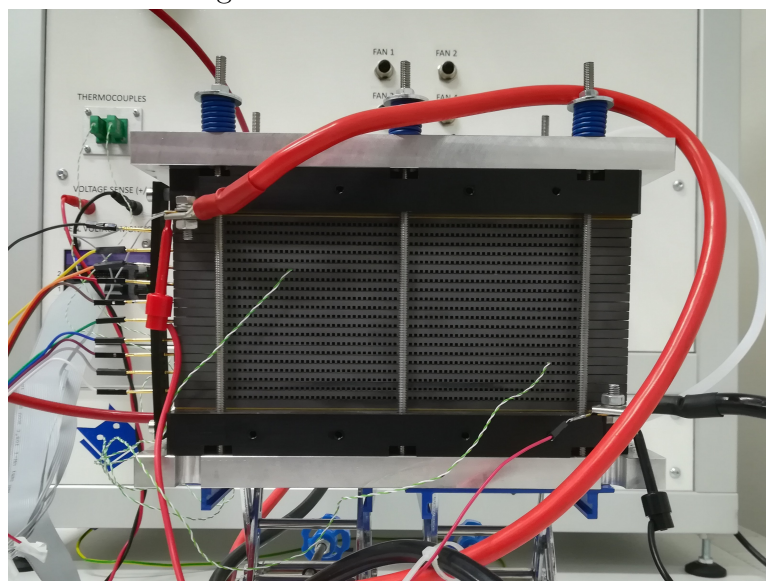
⁵For the controlling of the output of the cooling fans, we are using pulse-width modulation (PWM) and we will further characterize this power by the duty cycle D – that is, the fraction of one period during which the system is active. Unless said otherwise, whenever we mention the duty cycle, we mean the duty cycle of the cooling fans.

2. Measurement

2.1 Equipment

We are using an open-cathode, forced convection, dead-end mode (purging duration 500 ms and period 60 s) stack of 20 PEM fuel cells with the *MEA 7* from *Cantian Polymer Energy Limited*. The total active area of all the PEMs is 100 cm². The rough size of the channels is 1.3 mm depth and 1.4 mm width for the cathode and 0.4 mm depth and 1.1 mm width for the anode. The geometry is shown in fig. 2.2. The stack is shown in fig. 2.1.

Figure 2.1: Photo of the stack.



For the experiments, we are using the testing station *Open-Cathode Stack Tester OBT* from the company *LeanCat*, a thermographic camera *Bosch GTC 400 C Professional*, and 2 cooling fans *ebm-papst 8214 J/2NP-015*. Our hydrogen is from the *Linde* company with purity of 99.995 %.

As the ultrasonic water fog generator, we are using a piezoelement submerged in a water reservoir.

2.2 Building the Stack

First, we have hand-built the stack using 20 MEAs, 19 bipolar plates, 2 end plates, insulation, and 2 ventilator fans.

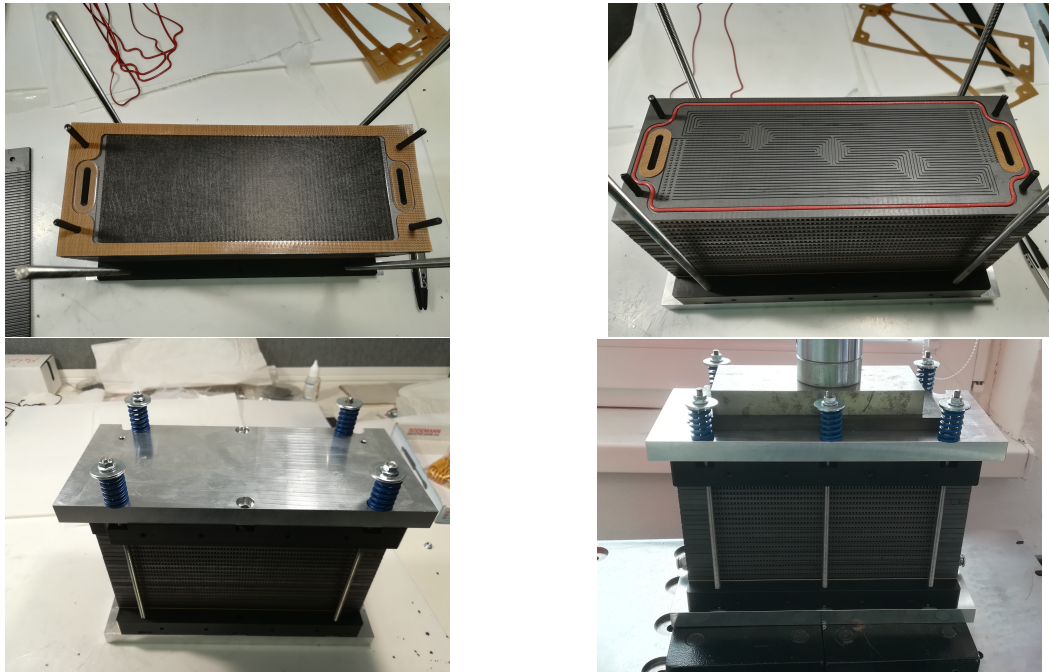
The stack had to be built very carefully as any imperfection in the placement of the the insulation can cause leakage of fuel.

To prevent this possibility, a leak-test has been performed before every measurement with the stack.

Photos from building the stack are shown in fig. 2.2.¹

¹Please note that the photos were taken not during the building of the stack that we were measuring with, but during building a second stack that ended up not being used. However, the process was very similar and these photos illustrate it equally well for both stacks.

Figure 2.2: Building the stack.



After assembling, the stack was compressed at about 30 times the atmospheric pressure and fixated by bolts, again, to seal the cells and prevent leakage.

2.3 Measurement Error

As the precision of the measurement devices was very high, almost the entire uncertainty in the measured current and power comes from variations in the experiment's conditions (unless said otherwise, voltage was controlled precisely and we are mostly concerned with the error in determining the current density).

One significant source of error came from reaching the steady state of operation. As noted earlier, we have taken at least 5 minutes after a voltage change in the measurement for the stack to settle. However, it is the case that in some of the measurements, the current was not yet completely constant when the measurement was taken.

We can estimate the magnitude of this error by looking at the characteristics at the time of measurement. Consider the figures 2.3 and 2.4. A measurement was taken at around the minute 22. From the properties of the measured characteristic, we can estimate the real value towards which the current converged, compare it to the measured value, and thus estimate the error.

The current measured there was 50.1 A. However, as we can see in 2.4, the current really converged to a value that could be as low as 49.5 A giving a relative error of 1.2 %. From this and similar analyses, we estimate that the error caused by this factor was around 2 %.

Another source of uncertainty can be seen in the very same picture – clearly, the current varied by as much as 1 A within the one-minute dead-end cycle (more on that below), which would cause another error of about 2 %. However, by considering the average value of the current within the one-minute window, which we tried to do, we estimate this factor to cause only about 1 % of relative error.

Figure 2.3: An example of the $I(t)$ dependency – full interval.

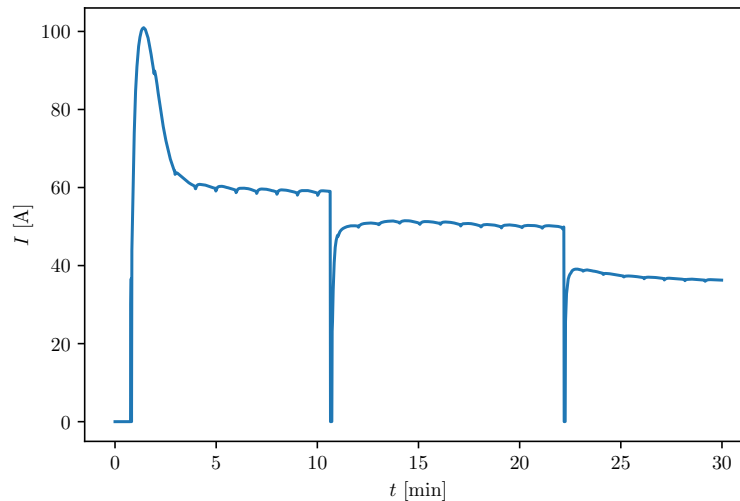
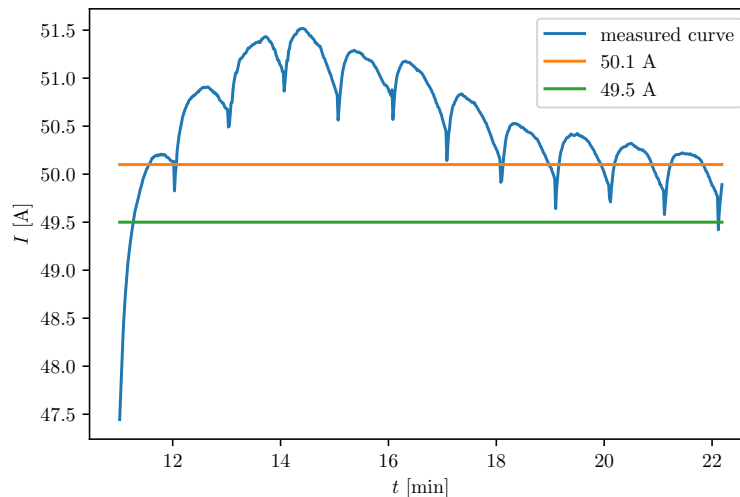


Figure 2.4: An example of the $I(t)$ dependency – close-up.



2.3.1 Uncertainty in Temperature

For most of our measurements, we have attempted to hold the temperature constant while measuring other characteristics. However, this task proved rather difficult as the temperature continued to fluctuate.

The core of the problem was inhomogeneity in the temperature throughout the stack. As noted earlier, we have used not one, but two thermocouples. On each of those, the temperature has been somewhat different. More importantly, though, the difference between these two temperatures has not been constant during the measurement, and thus it was impossible to hold both temperatures constant.

The temperatures throughout the measurements are shown in figures 2.5 to 2.7.²

²Because of the fluctuations and positioning of the thermocouples, we estimate the uncertainty in the measuring of temperatures on the thermocouples to be around 1 °C. Note that this is not the same as the error of measuring the “average” temperature of the stack.

Figure 2.5: Temperatures on the two thermocouples, 1st run of measurements.

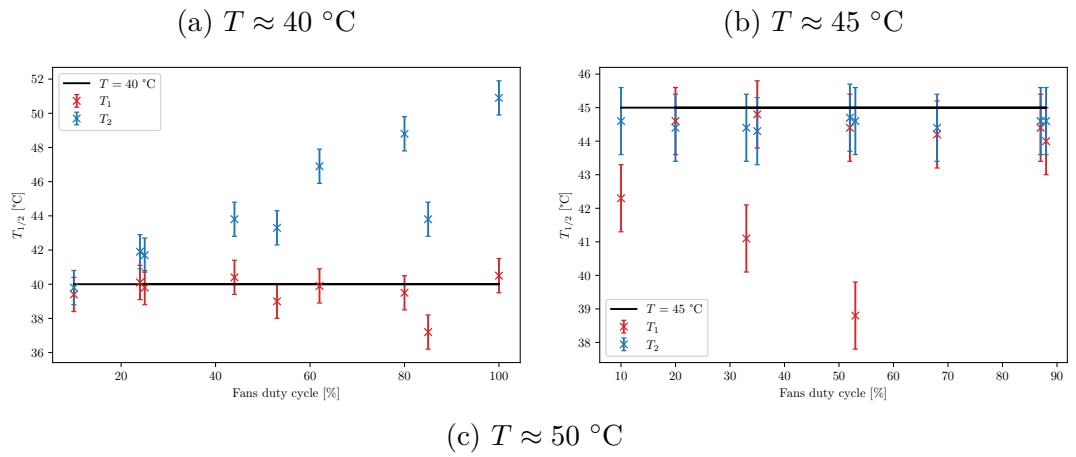


Figure 2.6: Temperatures on the two thermocouples, 2nd run of measurements.

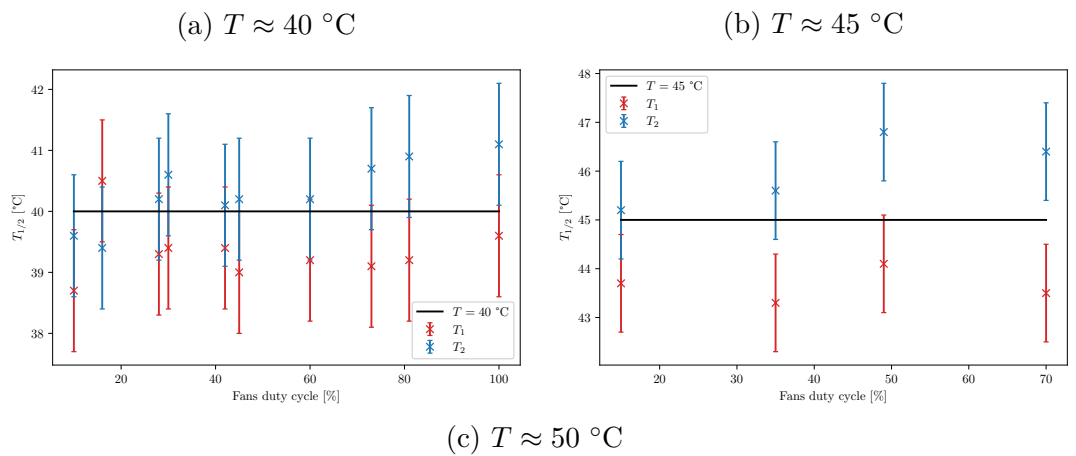
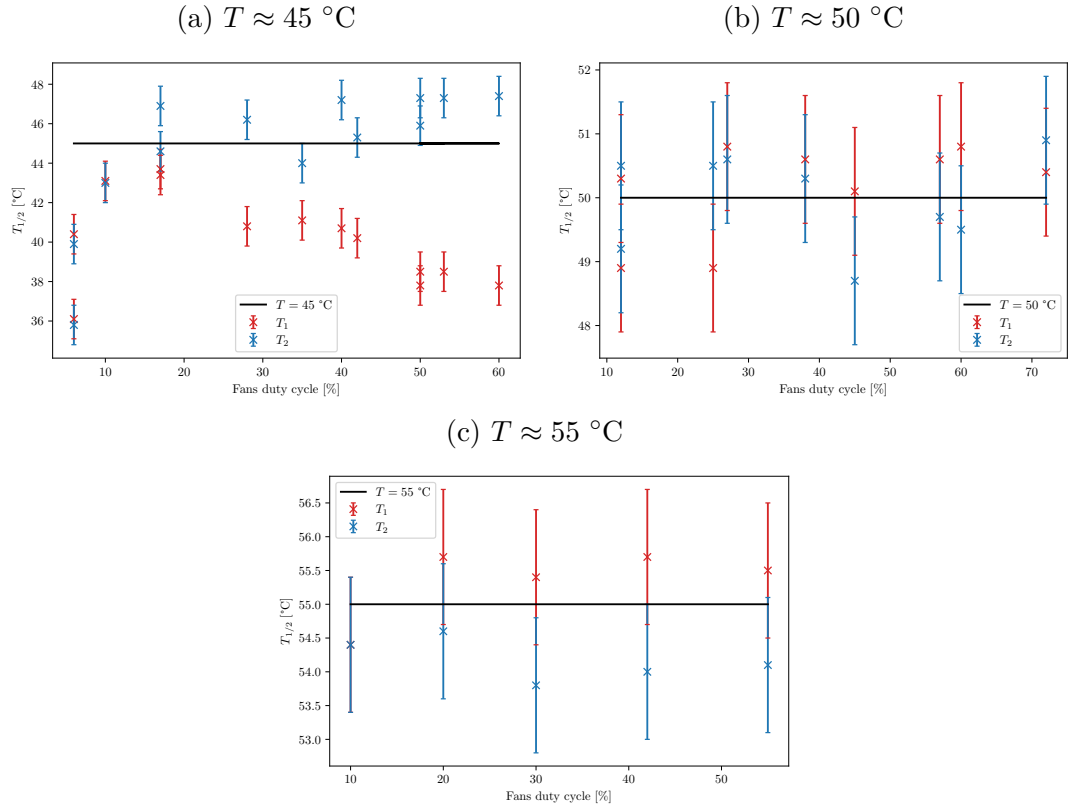


Figure 2.7: Temperatures on the two thermocouples, measurements with humidification.



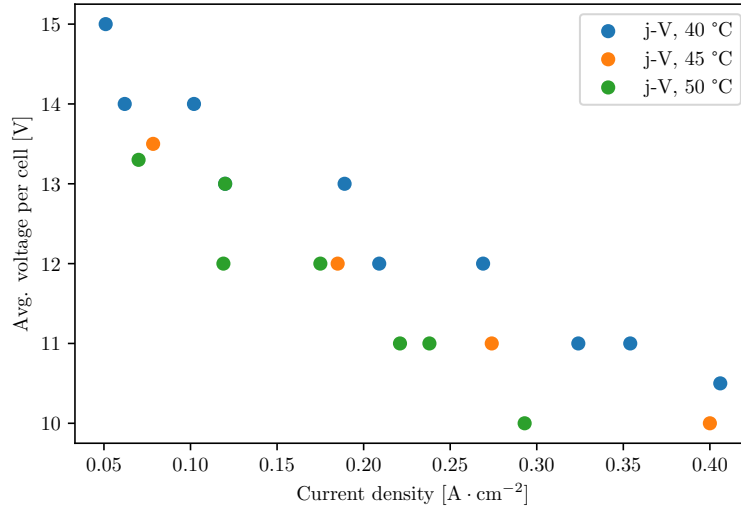
As we can see, for the second run of measurements and for most of the measurements with humidification, the temperatures stayed within the ± 2 °C range. Since the distinct measurements were taken at intervals 5 °C apart (40, 45, and 50 degrees without humidification and 45, 50, and 55 with humidification), these fluctuations in temperature do not render the measurements unusable.

We will concern ourselves with the 1st run of measurements shortly.

Consider the fig. 2.8 that shows the j - V characteristics (polarization curves) from the 2nd run of measurements.³ We can try to estimate the relative error caused by the stack temperature fluctuations and inhomogeneity from the average difference between the measured current densities at a given voltage for two different temperatures. Looking at the measurements at 11 V, we can estimate the difference at about $0.04 \text{ A} \cdot \text{cm}^{-2}$ around the value of current density $j = 0.28 \text{ A} \cdot \text{cm}^{-2}$, that is $1/7$ of the value. As noted earlier, the temperatures fluctuated by about 2 °C, while the spacing of the measurements is 5 °C. So, for our estimate we scale the $1/7$ by $2/5$ yielding $2/35$, or about 5.7 %. Repeating the procedure for several points, we estimate the relative error caused by this factor to be around 6.5 %.

³The methodology for obtaining these characteristics will be discussed later.

Figure 2.8: VA characteristics of the 2nd run of measurements.



2.3.2 Unusable Measurements

The influence of the temperature inhomogeneity can be seen on the following example.

During two of our earliest measurements, we were unable to properly control the temperatures and thus got the temperature differences shown in fig. 2.5 at 40 and 45 °C. The differences are clearly extreme, at the highest around 11 °C and 7 °C respectively. Note that we want to compare measurements that are 5 °C apart (40, 45, and 50 °C), but here we are getting differences that are much higher.

This discrepancy leads us to disregard these two measurements from further analysis. Note that to be consistent, we should also disregard the measurement with humidification at 45 °C, but for now, we will leave it in the analysis and comment on the reasons and consequences later.

One of the causes, apart from the fact that different parts of the stack were under slightly different load, as we will discuss later, might have been the fact that the ventilator fans had circular cross-section, and thus they likely did not cool every part of the stack equally, especially at high flow rates (which were used at high powers when vast amounts of waste heat were being produced).

2.3.3 Other Sources of Error and the Total Error

The performance of the stack highly depends on ambient conditions, which, although very similar in each of the experiments, were not controlled precisely.

We have approximated the influence of temperature fluctuations on the measurement error. However, many other factors, such as the temperature or humidity of the surrounding air cooling the fans, could have varied between the measurements, increasing the uncertainty.

As can be seen e.g. in fig. 2.8 in the measurement at 50 °C at 12 V, the values of current density differ even within measurements at one temperature (for most voltages, we have 2 measurements since we usually measured first from circa 14 down to 10 V and then back up), we roughly estimate the relative error of the

current measurement caused by this factor at 4 %.⁴

Putting all of the sources of error together⁵, we obtain the relative error of the current density as

$$\eta_j \approx \sqrt{2^2 + 1^2 + 6.5^2 + 4^2} \approx 8 \%. \quad (2.2)$$

Please note that this is still only a *rough estimate* of the total uncertainty as the influence of other variations or the correlations between the different sources of error were not taken into account.

2.4 Basic Characteristics

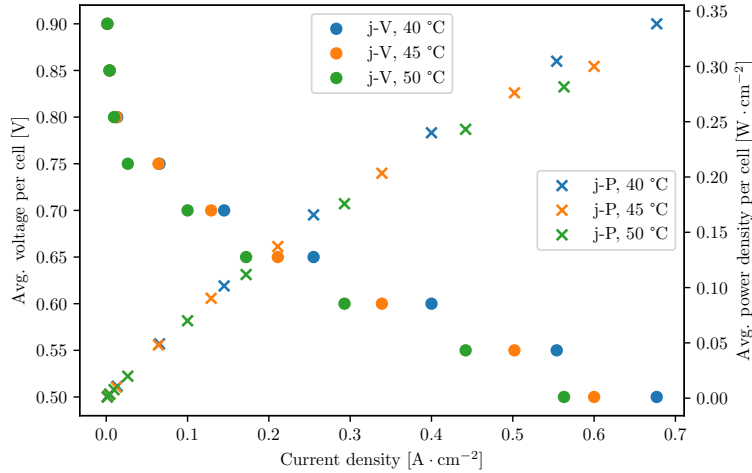
For the initial testing of the stack, we have measured several basic characteristics.

First, we have measured the j-V curve for three different temperatures – approx. 40, 45 and 50 °C.

During the measurement, the temperature was controlled by changing the duty cycle of the cooling fans.

The data are shown in the graph 2.9.

Figure 2.9: The j-V and j-P curves for different temperatures.



Note that these measurements were taken unfortunately only with one thermocouple and therefore they are inappropriate for comparing with further measurements since we cannot know how homogeneous the temperatures between the different parts of the stack were, which, as we have shown, has a large influence on the results. We are only including these characteristics as they illustrate the basic *shape* of the j-V (or j-P) curve well (further measurements that we will actually use for comparisons were taken in a more narrow range of voltages, which is not a problem for the further analysis, but they include mostly the linear part of the

⁴We arrived at this number via similar analysis to the one used for assessing the uncertainty caused by the temperature variations.

⁵The total relative error is

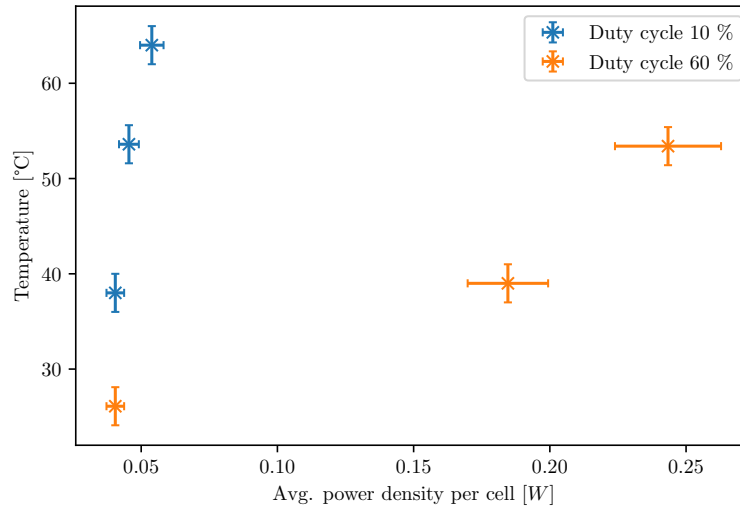
$$\eta = \sqrt{\sum_i \eta_i^2}, \quad (2.1)$$

where η_i are the constituent relative errors.

characteristic and do not show the entire curve). The errorbars are omitted in this figure not to clutter it.⁶

Next, we have measured the dependency of the temperature on the power produced by the stack for two different constant duty cycles of the cooling fan, 10 and 60 %. The measured data are shown in the fig. 2.10.

Figure 2.10: Dependency of the stack temperature on power for constant fan duty cycles.



Data shows that the temperature increases rapidly with increasing power as more waste heat is generated for higher power output. Also, the temperatures are lower for higher fan duty cycles as more air flows through and cools down the stack.

The influence of the dead-end mode can be seen in the measured data, see fig. 2.4 that shows the dependency of current on time during a part of one of our measurements. We observe that at the intervals where the current does not change rapidly, there is still some variation. More precisely, the current first rises, then falls again periodically as the water and nitrogen diffused through the membrane build up and clog the cell. Then, every minute, the current drops rapidly and then jumps back up again. This is the effect of purging, where every minute, the stack is cleared of waste products and thus can work more efficiently again.

2.5 Artificial Humidification via Piezoelement

As discussed previously, the performance of a stack is highly dependent on the humidity of the air, with higher humidity improving the performance (as long as they are low enough not to cause flooding).

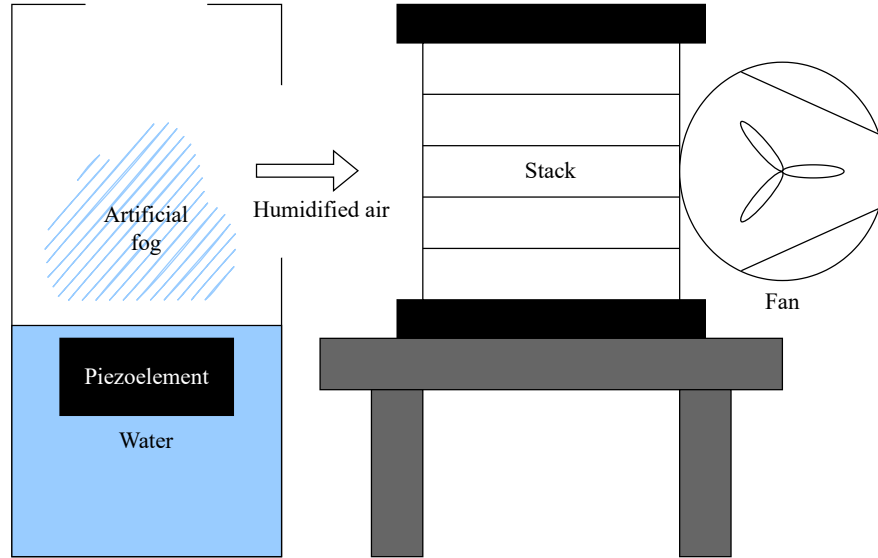
We have investigated a new method of artificial humidification of the incoming air and measured its influence on the stack performance and the efficiency of cooling.

⁶Also note that because of the lack of second voltage monitor, the relative uncertainty in current density would have to be larger than the aforementioned 8 %.

The humidification was achieved via a piezoelement submerged in a water reservoir next to the stack, which created an artificial “fog” that was then pulled into the stack via cooler fans (that normally serve for forced convection of the air into the stack).

The schema of the humidification system is shown in fig. 2.11.

Figure 2.11: Schema of the humidification system.



This method is much more energy-efficient than water evaporation by heating elements, yet much cheaper and simpler than classical external humidifiers (which are not feasible for open cathode systems), highly lowering the probability of malfunction.

2.6 Measuring the Efficiency of Cooling

To assess the efficiency of cooling, we have measured the P_{loss} as a function of the fan duty cycle while keeping the temperature constant⁷ in the following way: After setting a voltage, we have changed the duty cycle until a stable temperature was reached. After each voltage change, we have waited at least 5 minutes, even if the temperature has been stable, to ensure the stack has reached a steady state of operation.

For each datapoint, we have measured several characteristics – voltage, current, duty cycle, and, using two thermocouples, temperature of two different parts of the stack.

The measurement has been repeated twice without humidification for each of the three selected temperatures: 40, 45, and 50 °C. And then carried out again with humidification at 45, 50, and 55 °C.⁸ Note that the selected temperatures for the measurements with humidification differ from those without it, since the 40 °C temperature proved to be too low for proper functioning of the stack with humidification. The results are shown in fig. 2.12 to 2.15.

⁷Within ± 2 °C, as discussed previously.

⁸However, some of the measurements have been disregarded because of the temperature variations noted earlier.

Figure 2.12: The dependency of P_{loss} on duty cycle for $T \approx 40$ °C.

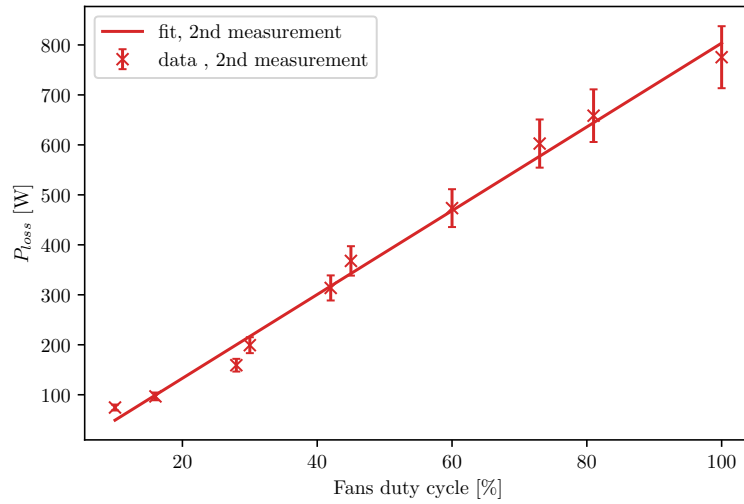


Figure 2.13: The dependency of P_{loss} on duty cycle for $T \approx 45$ °C.

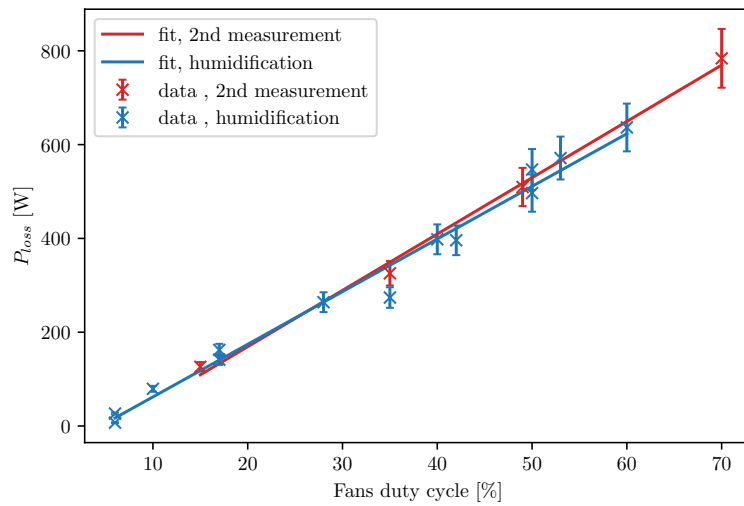


Figure 2.14: The dependency of P_{loss} on duty cycle for $T \approx 50$ °C.

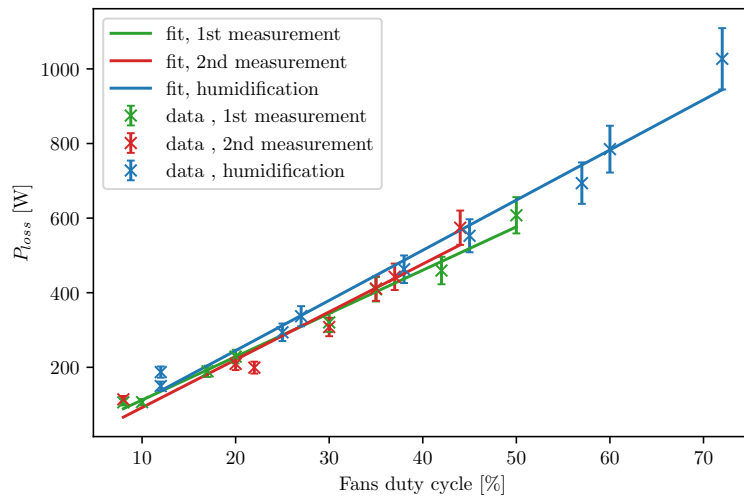
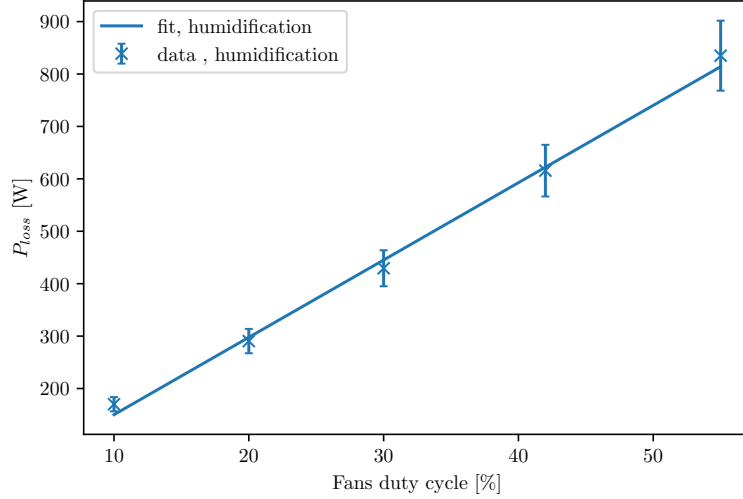


Figure 2.15: The dependency of P_{loss} on duty cycle for $T \approx 55$ °C.



For this work, the fits (obtained by least-squares linear regression) serve purely for easier visual comparison of the measurements, however, the fit parameters can in principle be used for mathematical modelling of the stack or better electronic operation control. Thus, we are including the values of all the fit parameters a and b in the dependency $P_{loss} = aD + b$ in the tables 2.1 and 2.2.⁹ The lower index in the parameter’s name indicates the measurement set to which the value belongs. The duty cycle here is given so that $D \in [0, 1]$.

Table 2.1: $P_{loss}(D)$ fit parameters “ a ”

T [°C]	$a_{1st}/100$ [W]	$a_{2nd}/100$ [W]	$a_{hum.}/100$ [W]
40	12.0(9)	8.4(5)	—
45	11(1)	13(1)	11.2(6)
50	11.5(9)	13(2)	13(1)
55	—	—	15(1)

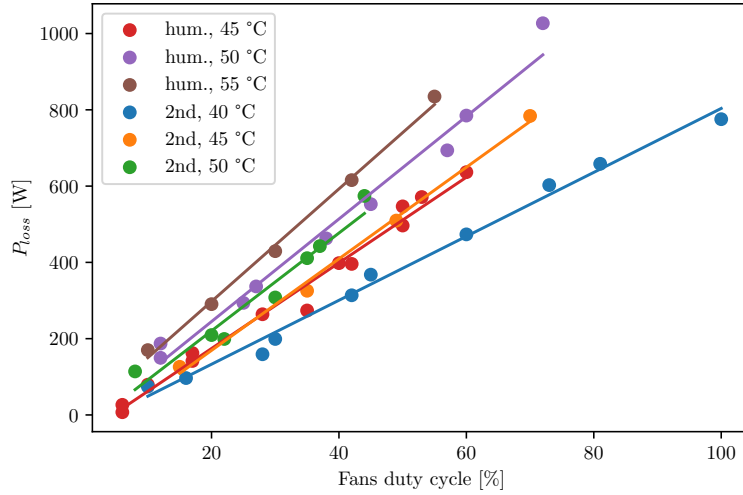
Table 2.2: $P_{loss}(D)$ fit parameters “ b ”

T [°C]	$b_{1st}/10$ [W]	$b_{2nd}/10$ [W]	$b_{hum.}/10$ [W]
40	−10(6)	−3(3)	—
45	−2(7)	−7(4)	−5(2)
50	−1(3)	−4(5)	−2(5)
55	—	—	0(5)

The fig. 2.16 shows the comparison of the measured dependencies. We are leaving out the first measurement at 50 °C for clarity and since it is very similar to the second measurement at this temperature.

⁹The errors for the parameters were obtained by Monte Carlo uncertainty propagation.

Figure 2.16: Comparison of $P_{loss}(D)$ dependencies for different temperatures.



2.6.1 Voltage Deviations

For the second measurement without humidification, and for all measurements with humidification, we have used 9-10 voltage monitor channels on different cells to measure the voltage differences among them. For technical reasons, only 9-10 voltage monitors were used for the 20 cell stack. The voltage on the channels has been distributed evenly among the relevant neighboring cells to obtain the approximation of the actual voltage on each cell.

The results are shown in figures 2.17 to 2.22 in the form of color maps plotted as cell index vs average power density (per cell) produced by the stack with color indicating the deviation as a percentage of the average cell voltage.

Note that the vertical lines dividing the x-axis are not equidistant since each interval between two of them represents one of the measurements, which were not equidistant in power density. For better comparison, all of these graphs have the same ranges on all axes, except for color for the 45 °C measurement with humidification, which exhibits far higher variations in cell voltages than the other measurements.

Figure 2.17: Deviations of cell voltages from the mean for $T \approx 40$ °C.

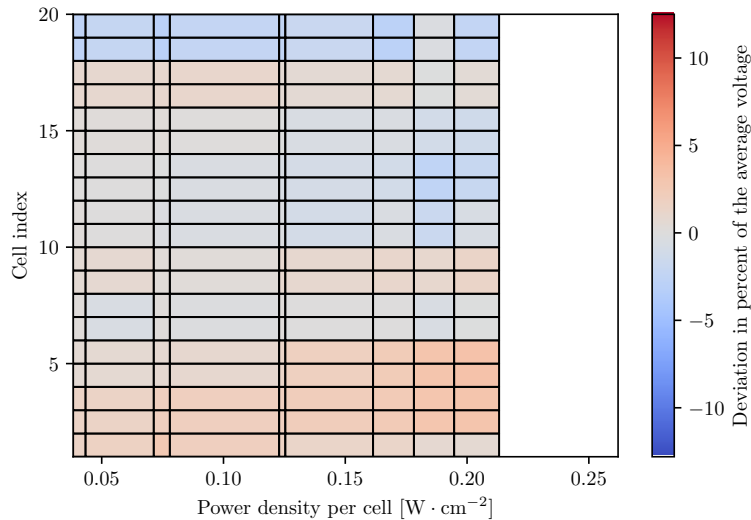


Figure 2.18: Deviations of cell voltages from the mean for $T \approx 45 \text{ }^\circ\text{C}$.

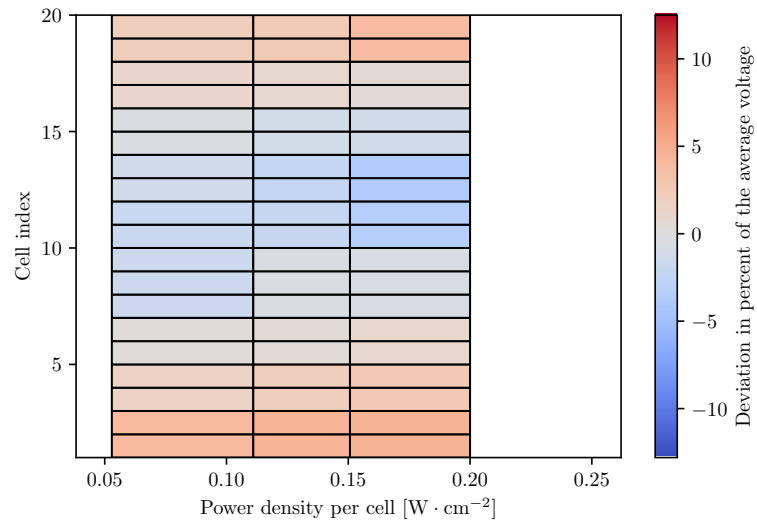


Figure 2.19: Deviations of cell voltages from the mean for $T \approx 50 \text{ }^\circ\text{C}$.

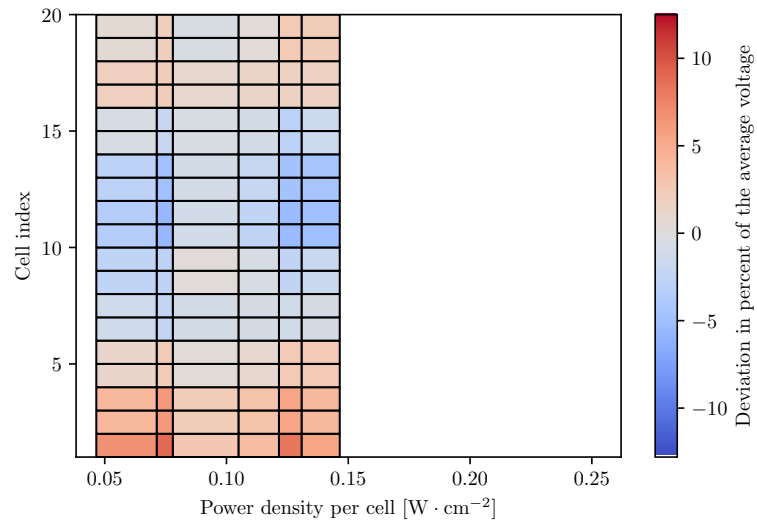


Figure 2.20: Deviations of cell voltages, $T \approx 45 \text{ }^\circ\text{C}$, with humidification.

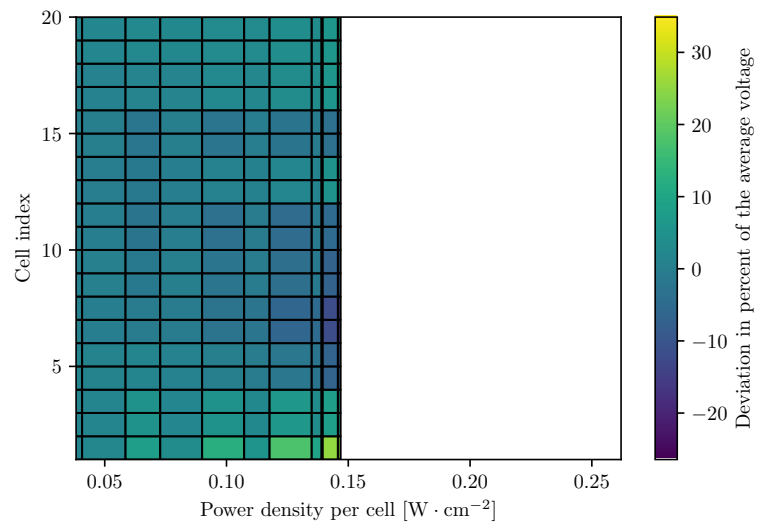


Figure 2.21: Deviations of cell voltages, $T \approx 50 \text{ }^\circ\text{C}$, with humidification.

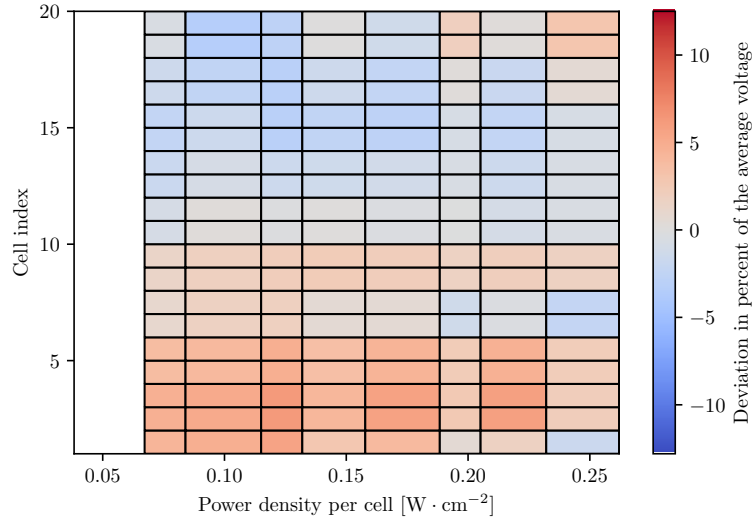
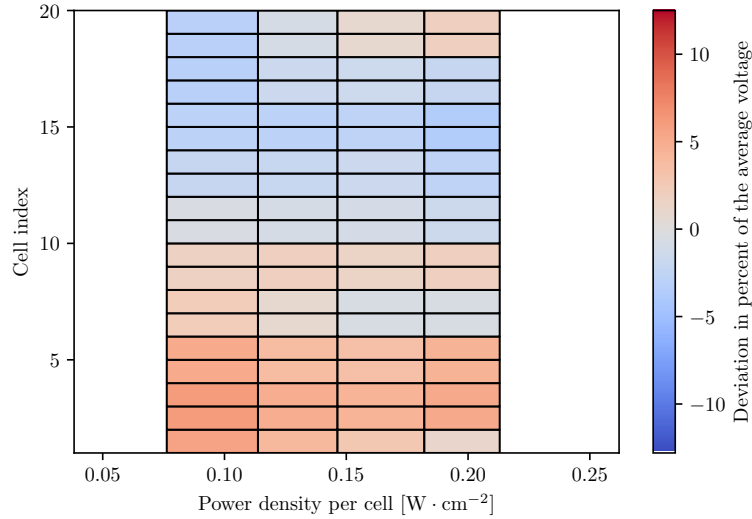


Figure 2.22: Deviations of cell voltages, $T \approx 55 \text{ }^\circ\text{C}$, with humidification.



In the $45 \text{ }^\circ\text{C}$ measurement with humidification, the difference between largest and lowest voltage is almost 70 % of the average cell voltage. That is in line with the fact that this measurement has the lowest voltage and power density for a given current density of all the measurements. It is very likely that the low temperature was insufficient for optimal evaporation and the stack was flooded.

Looking at the data more closely, see fig. 2.23, we see that the extreme variances are present only for the three to five highest power loads. This might be because these loads also came with the highest fan power for cooling and therefore the largest amount of fog pulled into the stack. We suspect this caused extreme flooding in some, but not all, of the cells, causing large voltage variations.

The fig. 2.24 shows the standard deviations of the cell voltages for different powers produced.¹⁰ We observe a slight positive correlation between the power output and the deviations for most of the measurements. The fig. 2.25 shows the same, but without the measurement with humidification at $45 \text{ }^\circ\text{C}$.

¹⁰We neglect the errorbars here not to clutter the figure more than is necessary.

Figure 2.23: Deviations of cell voltages $T \approx 45 \text{ }^\circ\text{C}$ with humidification close-up.
 (a) Lower power densities. (b) Higher power densities.

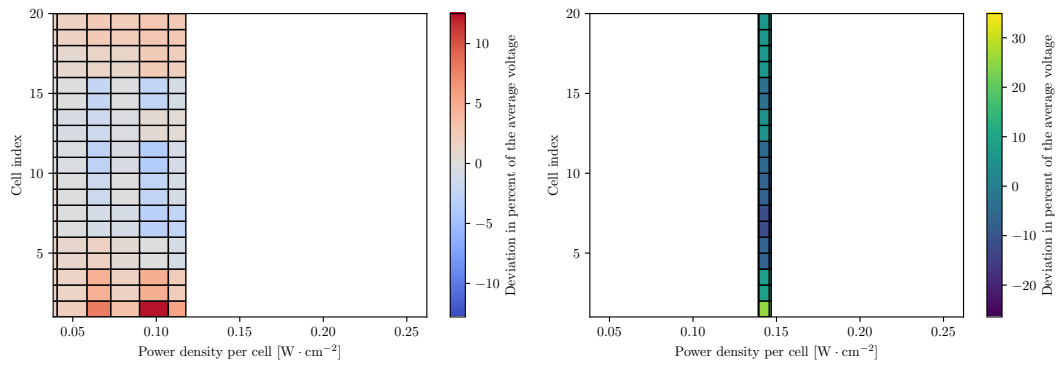


Figure 2.24: Average deviations in cell voltages.

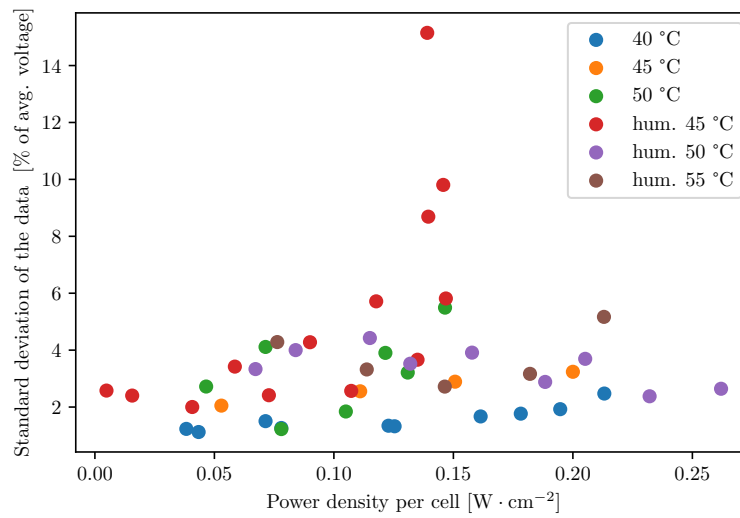
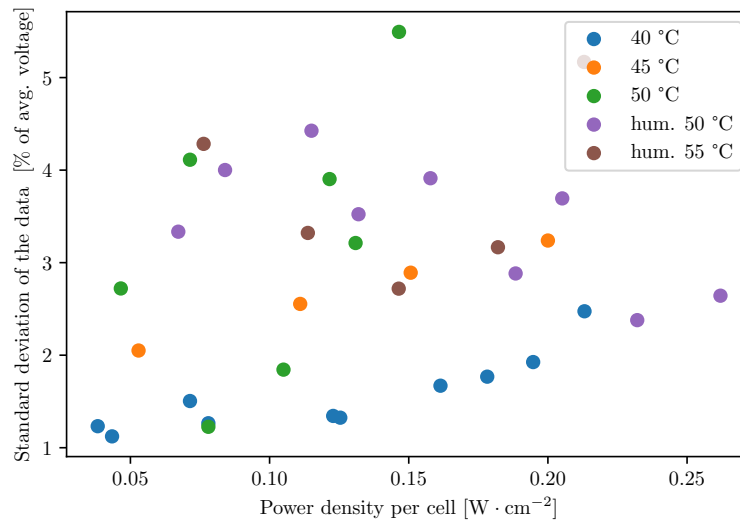


Figure 2.25: Average deviations in cell voltages without the extreme value.



2.7 Comparison – With and Without Humidification

The figures 2.26 and 2.27 show the comparison of all the measured j-V and j-P characteristics. We show the errorbars only for a few measurements, not to clutter the image.

Figure 2.26: Comparison of all the j-V characteristics.

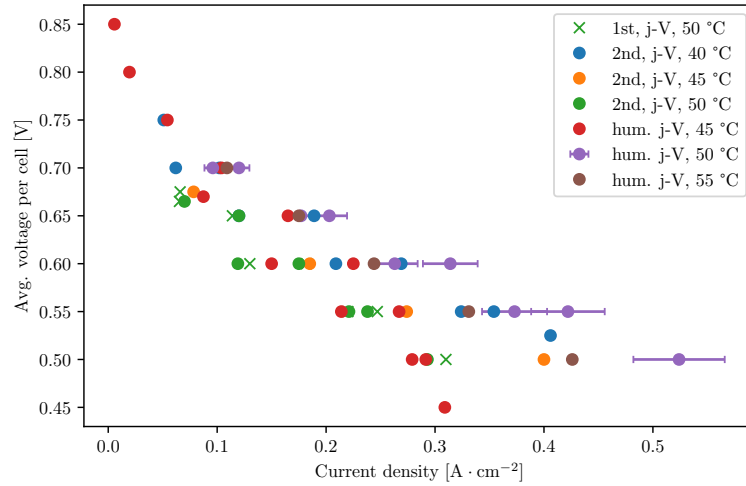
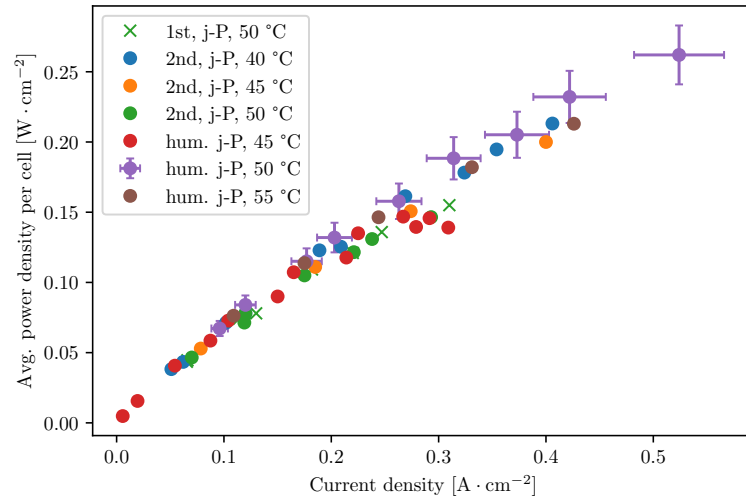


Figure 2.27: Comparison of all the j-P characteristics.



2.8 Thermal Maps of the Stack

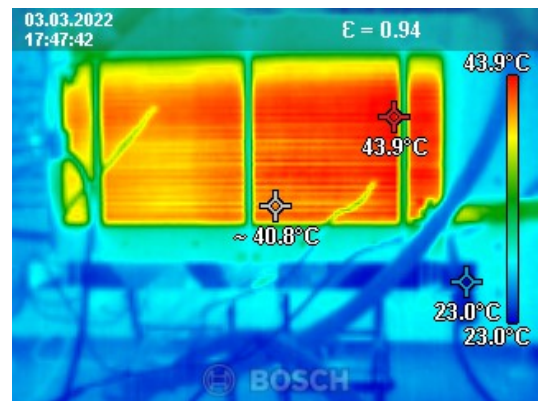
During the 2nd measurement without humidification at 45 °C, for each voltage, a thermal map of the stack was taken using a thermographic camera. The maps are shown in the figure 2.28. Note the temperatures at the thermal maps are lower than those given by the thermocouples since the thermocouples are inserted inside the stack, where the temperature is somewhat higher.

During the whole measurement, the temperature differences between different parts of the stack were around 3 – 4 °C, or, up to 10 %.

Figure 2.28: Thermal maps for $T \approx 45$ °C.

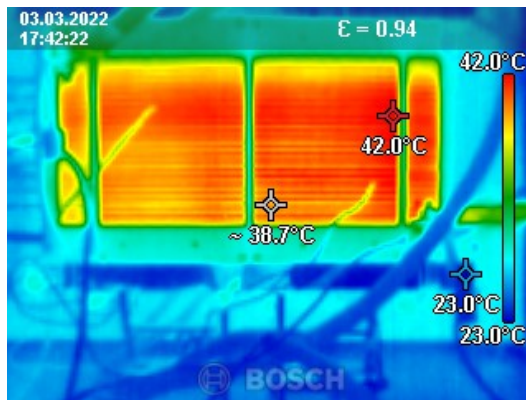
(a) 10 V

(b) 11 V



(c) 12 V

(d) 13.5 V



3. Discussion of the Results

3.1 Basic Characteristics

The measured j-V and j-P characteristics are in good agreement with the common characteristics for fuel cells [7].

The measurement of dependency of the stack temperature on power (see fig. 2.10) is in line with the expectation that for higher power production, the stack produces more waste heat and therefore the temperature is higher. Also, for higher fan power, the stack is cooled more efficiently and thus the temperature is lower than in the case of lower fan power.

3.2 Voltage Deviations

It should be noted that the variances in voltages on different cells shown in figures 2.17 to 2.22 must be interpreted as lower bounds for the actual variances, since we had less voltage monitor channels than we had cells and thus to estimate the voltage on all the cells, we had to take the averages for neighboring 1 – 3 cells.

The deviations mostly stayed within 8 % of the average cell voltage (and, except for the 45 °C measurement, all voltages stayed within 13 %). For comparison, different articles have found the differences around 5 – 16 % for different conditions and loads [25, 26, 27].

3.3 Systematic and Statistical Error

So far, we only concerned ourselves with the systematic error of each measurement. As noted earlier, the estimation of the systematic error is rather difficult as many factors play a role. For better quantification of the error, it would be highly preferred to perform multiple measurements for each of the conditions (e.g. at a given temperature with and without humidification) and to quantify the statistical error. Unluckily, repeating the experiment many times was not possible for this work given the long duration of each measurement.¹

3.4 Power Lost to Heat and Cooling

Let us now consider the power lost by the stack once more. There are several factors influencing this loss, in general

$$P_{loss} = P_{vent} + P_{rad} + P_{add.heat} , \quad (3.1)$$

where P_{vent} is the heat power that the air ventilates from the stack, P_{rad} is the power lost to radiation, and $P_{add.heat}$ is additional power in heat that the stack produces but is not ventilated and thus heats up the stack.

¹We have repeated the measurements without humidification, but had to disregard two thirds of them for reasons discussed earlier. The measurement at 50 °C that was actually carried out twice without problems with temperature non-uniformity, shows internal consistency between the two runs.

Let us look at the different summands. The power lost to radiation is, by the Stefan-Boltzmann law,

$$P_{rad} = S\sigma T^4, \quad (3.2)$$

where $\sigma = 5.6704 \cdot 10^{-8} \text{ W} \cdot \text{m}^{-2}\text{K}^{-1}$ is the Stefan-Boltzmann constant. For the temperature $T \approx 300 \text{ K}$ and the surface area of the stack $S \approx 0.07 \text{ m}^{-2}$ this gives $P_{rad} \approx 40 \text{ W} \cdot \text{s}^{-1}$.

We will neglect this summand as it is independent of the duty cycle and thus only contributes as a constant shift in the $P_{loss}(D)$ characteristics that we measured.

The power heating up the stack is

$$P_{add.heat} = \frac{dQ}{dt} = mc \frac{dT}{dt}. \quad (3.3)$$

Thus, if we keep the temperature constant, the eq. (3.1) reduces to

$$P_{loss} \approx P_{vent}. \quad (3.4)$$

Considering this, it makes perfect sense that all of the relationships between P_{loss} and duty cycle exhibit a linear dependency (see fig. 2.16) – the duty cycle is directly proportional to the amount of the air going through the stack while the P_{vent} is the amount of heat power that the air “clears out” of the stack.

Generally, more efficient cooling has been observed for higher temperatures both with and without humidification.²

3.5 The Effects of Humidification

From the figures 2.13 and 2.14, we see that the cooling efficiency remained essentially unchanged after the introduction of the humidification via piezoelement. And, as can be seen on fig. 2.25, humidification likely had little effect on the voltage differences among different cells.

Consider the figures 2.26 and 2.27. We can see that the measurement with humidification at 50 °C slightly outperformed all of the other measurements, with and without humidification.

Further note that the measurements at 50 °C without humidification are consistent with each other and that the measurement at the same temperature with humidification outperforms them significantly.

For the measurements without humidification, the lower the temperature, the better the performance. This suggest that higher temperatures have led to dry-out of the membrane. This is further consistent with the fact that for the measurement at 50 °C, humidification improved performance.

As for the measurement at 55 °C with humidification, it exhibits a lower performance than several other measurements. This may suggest that, even with humidification, this temperature is high enough to cause dry-out.

For future work, it would be desirable to control the power of the piezoelement and to investigate different intensities of fog production to ensure optimal humidification without flooding.

²See fig. 2.16 – the higher the $P_{loss} \approx P_{vent}$ is for constant duty cycle, the more waste heat is cleared out meaning higher cooling efficiency.

3.5.1 Additional Weight Added by Humidification System

As for the additional weight this system would bring, we have not measured the water consumption of the system precisely (as optimizing the technology is much more pressing) but we can make a rough estimate. We have used a container of water of about circular cross-section and a diameter of about 15 cm. During a three-hour run of the system, the surface has not decreased by more than 2 mm, this simply gives the consumption as

$$\text{water consumption} \approx \frac{\pi \left(\frac{15 \text{ cm}}{2}\right)^2 (2 \text{ mm})}{3 \text{ h}} \approx 12 \text{ ml} \cdot \text{h}^{-1}, \quad (3.5)$$

which is a rather small additional weight needed. The piezoelement itself would likely weigh significantly more than water needed for operation.

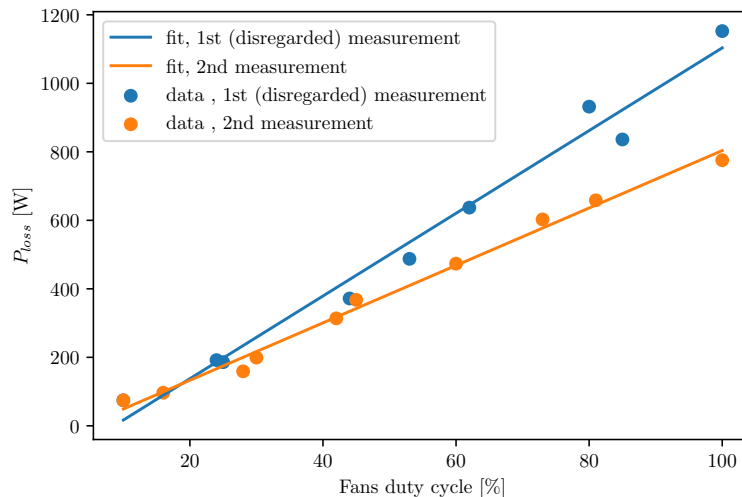
3.6 The Disregarded Measurements

Let us now go back to the measurements we disregarded earlier: 40 and 45 °C without humidification.

For the 40 °C measurement, the differences in the temperatures were fixed near the end of the measurement simply by slightly moving the thermocouple, suggesting that the problem was a bad contact and that the real temperature of the stack had been very different than recorded during the measurement.

To illustrate the effects of the temperature discrepancy, consider the cooling efficiency measurement for 40 °C and compare the 1st (disregarded) and 2nd measurement as shown in fig. 3.1.

Figure 3.1: Comparison of $P_{loss}(D)$ characteristics of the 1st (disregarded) and 2nd 40 °C measurements without humidification.



There is a rather large difference between the two, and, perhaps more importantly, it increases with the difference between the temperatures on the thermocouples in the disregarded measurement (the differences in temperatures on the thermocouples in the second measurement are much smaller).

Thus, we attribute the differences between the two measurements to the imperfect conditions in the first measurement and disregard it.

In all of the subsequent measurements, we made sure the thermocouples have a good contact with the stack. Thus, there was a much higher certainty of keeping constant temperature throughout the measurement. And so, the 2nd round of measurements and the measurements with humidification were carried out at conditions more similar to each other than to the first set of measurements.

We should also compare the j-V curves of those disregarded measurements with the rest. This is done in the figures 3.2 and 3.3. Here, we see that the two disregarded measurements actually outperform all of the other measurements! Further note, that these two are highly inconsistent with the corresponding measurements carried out at the same temperature (see e.g. the 1st vs 2nd measurement at 45 °C).

Figure 3.2: Comparison of all the j-V characteristics, including the disregarded ones.

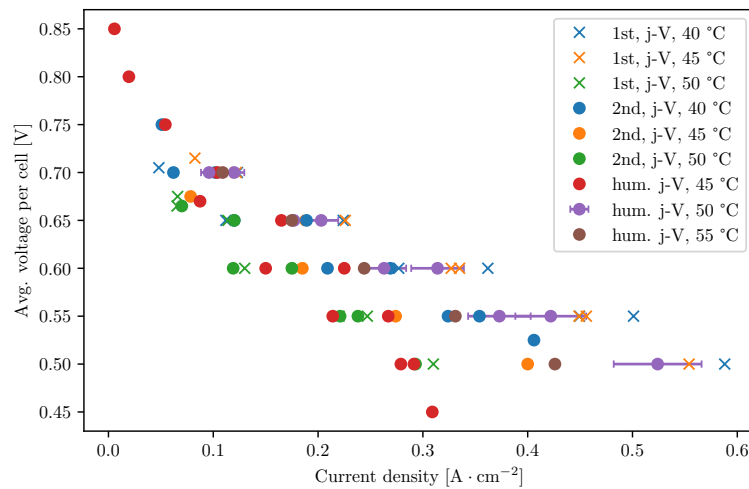
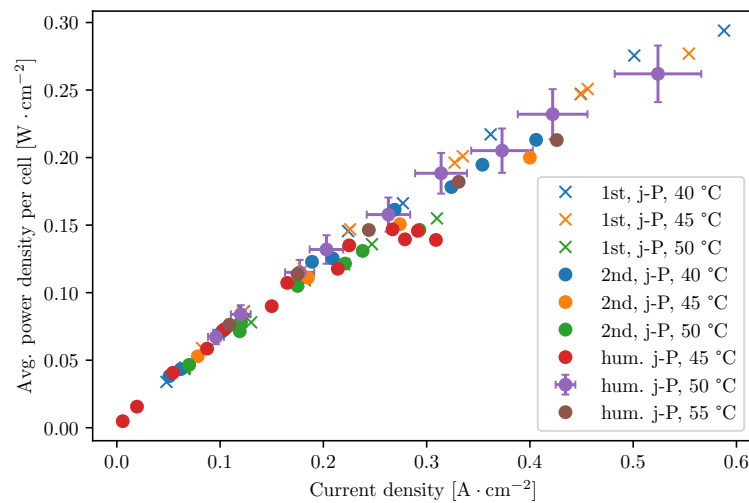


Figure 3.3: Comparison of all the j-P characteristics, including the disregarded ones.



One reason for the discrepancy might simply be the timing – the two disregarded measurements were taken at least a month before the rest, during which time the stack might have endured further degradation.

Given the highly fluctuating and badly controlled conditions in the first run of measurements, we do sincerely believe that these should be disregarded/cannot be meaningfully compared to the rest of the measurements. However, we include this comparison not to fall for cherry-picking.

Note that even if the conditions were sufficiently similar for these comparisons to make sense, which we do not believe to be the case, the fact would still remain that the humidification highly improved performance for the 50 °C run.

In any case, further thorough investigation is needed to establish the practical utility of this humidification method.

3.6.1 The 45 °C Humidification Measurement

For consistency, it may seem we should have also disregarded the measurement with humidification at 45 °C. However, this measurement was carried out while controlling the temperature more closely, which suggests a higher reliability of the temperature readings.

The high differences between the temperatures in this case are likely to be caused by very high levels of flooding non-uniformly throughout the stack, which also came with large variances of voltage between the cells, see fig. 2.23.

This can also be seen on the j-V and j-P curves 2.26 and 2.27, where this measurement exhibits the second worst overall performance and also very high differences between the measured current densities at the same voltage a few hours apart.

It is interesting to note, though, that the cooling efficiency curve has not changed, see fig. 2.13.

Conclusion

We have hand-built a PEMFC stack of 20 cells and measured its basic characteristics such as the j-V and j-P curves as well as the dependency of the temperature of the stack on the power produced by the stack for constant duty cycle of the cooling fans. These basic characteristics were in line with the commonly known theoretical and experimental characteristics of PEMFC hydrogen fuel cell stacks.

We have implemented and tested the performance of a new method for water and thermal management – the humidification of the air via the use of piezoelement submerged in water.

To assess the effect of this method on cooling efficiency, we have measured the dependency of power lost by the stack on the duty cycle of the cooling fans for approximately constant temperatures, with and without humidification. All of these relationships exhibit linear dependency. The humidification had little to no effect on the cooling efficiency. A more efficient cooling has been observed for higher temperatures both with and without humidification.

We have measured the voltage variations between different cells, which were again not changed significantly after the introduction of humidification, and, for the vast majority of measurements, stayed within the range of 6 – 12 %.

The dependencies of voltage and power density on the current density were also measured. Without humidification, the lower the temperature, the better the performance of the stack, suggesting higher temperatures led to dry-out.

The best performance among all the measurement was observed for 50 °C with humidification. Said measurement outperformed the characteristics at the same temperature without humidification significantly. A concern was raised about the possibility of a different measurement, carried out at different conditions, outperforming the mentioned best one.

A gross estimate of additional weight needed for carrying the water has been made at modest $12 \text{ ml} \cdot \text{h}^{-1}$.

Our results suggest a possible potential of the new humidification method, but are not decisive. For further research, measuring the j-V characteristics for different intensities of cooling (or powers of the piezoelement) is desirable. This would allow to find an optimal level of humidification for a given temperature (or other conditions).

Bibliography

- [1] Max Roser Hannah Ritchie and Pablo Rosado. Energy. *Our World in Data*, 2020. <https://ourworldindata.org/energy>.
- [2] Ingrid Torjesen. Fossil fuel air pollution blamed for 1 in 5 deaths worldwide. *BMJ*, 372, 2021.
- [3] Nikolaos S. Thomaidis, Francisco J. Santos-Alamillos, David Pozo-Vázquez, and Julio Usaola-García. Optimal management of wind and solar energy resources. *Computers and Operations Research*, 66:284–291, 2016.
- [4] P.P. Edwards, V.L. Kuznetsov, W.I.F. David, and N.P. Brandon. Hydrogen and fuel cells: Towards a sustainable energy future. *Energy Policy*, 36(12):4356–4362, 2008. Foresight Sustainable Energy Management and the Built Environment Project.
- [5] Jundika C. Kurnia, Benitta A. Chaedir, Agus P. Sasmito, and Tariq Shamim. Progress on open cathode proton exchange membrane fuel cell: Performance, designs, challenges and future directions. *Applied Energy*, 283:116359, 2021.
- [6] Ainhoa de las Heras Jiménez, Francisco José Vivas Fernández, Francisca Segura Manzano, Manuel Joaquín Redondo González, José Manuel Andújar Márquez, et al. Air-cooled fuel cells: Keys to design and build the oxidant/cooling system.
- [7] R. O’Hayre, S.W. Cha, W. Colella, and F.B. Prinz. *Fuel Cell Fundamentals*. Wiley, 2016.
- [8] Jaeman Park, Hwanyeong Oh, Yoo Il Lee, Kyoungdoug Min, Eunsook Lee, and Jy-Young Jyoung. Effect of the pore size variation in the substrate of the gas diffusion layer on water management and fuel cell performance. *Applied Energy*, 171:200–212, 2016.
- [9] Zi’ang Xiong, Shijun Liao, Dai Dang, Xinlong Tian, Sanying Hou, Fangfang Liu, Hongliang Peng, and Zhiyong Fu. Enhanced water management in the cathode of an air-breathing pemfc using a dual catalyst layer and optimizing the gas diffusion and microporous layers. *International Journal of Hydrogen Energy*, 40(10):3961–3967, 2015.
- [10] Stephan Strahl, Attila Husar, and Alejandro A. Franco. Electrode structure effects on the performance of open-cathode proton exchange membrane fuel cells: A multiscale modeling approach. *International Journal of Hydrogen Energy*, 39(18):9752–9767, 2014.
- [11] Denise A. McKahn. Influence of gas channel depth in self-humidified miniature pem fuel cells with dead-ended anode. *International Journal of Hydrogen Energy*, 40(22):7168–7181, 2015.
- [12] Fereshteh Salimi Nanadegani, Ebrahim Nemati Lay, and Bengt Sunden. Effects of an mpl on water and thermal management in a pemfc. *International Journal of Energy Research*, 43(1):274–296, 2019.

- [13] Akira Nishimura, Satoru Kamiya, Tatsuya Okado, Yusuke Sato, Masafumi Hirota, and Mohan Lal Kolhe. Heat and mass transfer analysis in single cell of pefc using different pem and gdl at higher temperature. *International Journal of Hydrogen Energy*, 44(56):29631–29640, 2019. The 2nd International Symposium on Hydrogen Energy and Energy Technologies (HEET-2018).
- [14] Young-Jun Sohn, Sung-Dae Yim, Gu-Gon Park, Minjin Kim, Suk-Won Cha, and Kyoungyoun Kim. Pemfc modeling based on characterization of effective diffusivity in simulated cathode catalyst layer. *International Journal of Hydrogen Energy*, 42(18):13226–13233, 2017.
- [15] Francesco Valle. *Electrocatalyst degradation in high temperature PEM fuel cells*. PhD thesis, 04 2015.
- [16] Jih-Sheng Lai and Michael W. Ellis. Fuel cell power systems and applications. *Proceedings of the IEEE*, 105(11):2166–2190, 2017.
- [17] Deryn Chu and Rongzhong Jiang. Comparative studies of polymer electrolyte membrane fuel cell stack and single cell. *Journal of Power Sources*, 80(1):226–234, 1999.
- [18] Quentin Meyer, Ahmed Himeur, Sean Ashton, Oliver Curnick, Ralph Clague, Tobias Reisch, Paul Adcock, Paul R. Shearing, and Daniel J.L. Brett. System-level electro-thermal optimisation of air-cooled open-cathode polymer electrolyte fuel cells: Air blower parasitic load and schemes for dynamic operation. *International Journal of Hydrogen Energy*, 40(46):16760–16766, 2015.
- [19] M. Miller and A. Bazylak. A review of polymer electrolyte membrane fuel cell stack testing. *Journal of Power Sources*, 196(2):601–613, 2011.
- [20] Ben Chen, Wandu Ke, Maji Luo, Jun Wang, Zhengkai Tu, Mu Pan, Haining Zhang, Xiaowei Liu, and Wei Liu. Operation characteristics and carbon corrosion of pemfc (proton exchange membrane fuel cell) with dead-ended anode for high hydrogen utilization. *Energy*, 91:799–806, 2015.
- [21] Leonard J. Bonville, H. Russell Kunz, Ying Song, Anthony Mientek, Minkmas Williams, Albert Ching, and James M. Fenton. Development and demonstration of a higher temperature pem fuel cell stack. *Journal of Power Sources*, 144(1):107–112, 2005.
- [22] Yangyang Chen, Qifei Jian, Zhe Huang, Jing Zhao, Xingying Bai, and Deqiang Li. Improvement of thermal management of proton exchange membrane fuel cell stack used for portable devices by integrating the ultrathin vapor chamber. *International Journal of Hydrogen Energy*, 46(74):36995–37006, 2021.
- [23] Agus P. Sasmito, Jundika C. Kurnia, Tariq Shamim, and Arun S. Mujumdar. Optimization of an open-cathode polymer electrolyte fuel cells stack utilizing taguchi method. *Applied Energy*, 185:1225–1232, 2017. Clean, Efficient and Affordable Energy for a Sustainable Future.

- [24] K W Harrison, R Remick, A Hoskin, and G D Martin. Hydrogen production: Fundamentals and case study summaries; preprint. 1 2010.
- [25] Wenhua H. Zhu, Robert U. Payne, Donald R. Cahela, and Bruce J. Tatarchuk. Uniformity analysis at mea and stack levels for a nexa pem fuel cell system. *Journal of Power Sources*, 128(2):231–238, 2004.
- [26] Paul Rodatz, Felix Büchi, Chris Onder, and Lino Guzzella. Operational aspects of a large pefc stack under practical conditions. *Journal of Power Sources*, 128(2):208–217, 2004.
- [27] S Giddey, F.T Ciacchi, and S.P.S Badwal. Design, assembly and operation of polymer electrolyte membrane fuel cell stacks to 1 kwe capacity. *Journal of Power Sources*, 125(2):155–165, 2004.

List of Figures

1.1	Schema of a PEMFC fuel cell.	4
1.2	Micro-structure modeling of the agglomerate catalyst layer [from 14].	5
1.3	A typical polarization curve of a PEM fuel cell [taken from 15].	5
1.4	Designs of PEMFC systems: (a) typical and (b) open cathode system [taken from 5].	7
1.5	Schema of an open-cathode stack.	7
2.1	Photo of the stack.	10
2.2	Building the stack.	11
2.3	An example of the $I(t)$ dependency – full interval.	12
2.4	An example of the $I(t)$ dependency – close-up.	12
2.5	Temperatures on the two thermocouples, 1st run of measurements.	13
2.6	Temperatures on the two thermocouples, 2nd run of measurements.	13
2.7	Temperatures on the two thermocouples, measurements with humidification.	14
2.8	VA characteristics of the 2nd run of measurements.	15
2.9	The j-V and j-P curves for different temperatures.	16
2.10	Dependency of the stack temperature on power for constant fan duty cycles.	17
2.11	Schema of the humidification system.	18
2.12	The dependency of P_{loss} on duty cycle for $T \approx 40$ °C.	19
2.13	The dependency of P_{loss} on duty cycle for $T \approx 45$ °C.	19
2.14	The dependency of P_{loss} on duty cycle for $T \approx 50$ °C.	19
2.15	The dependency of P_{loss} on duty cycle for $T \approx 55$ °C.	20
2.16	Comparison of $P_{loss}(D)$ dependencies for different temperatures.	21
2.17	Deviations of cell voltages from the mean for $T \approx 40$ °C.	21
2.18	Deviations of cell voltages from the mean for $T \approx 45$ °C.	22
2.19	Deviations of cell voltages from the mean for $T \approx 50$ °C.	22
2.20	Deviations of cell voltages, $T \approx 45$ °C, with humidification.	22
2.21	Deviations of cell voltages, $T \approx 50$ °C, with humidification.	23
2.22	Deviations of cell voltages, $T \approx 55$ °C, with humidification.	23
2.23	Deviations of cell voltages $T \approx 45$ °C with humidification close-up.	24
2.24	Average deviations in cell voltages.	24
2.25	Average deviations in cell voltages without the extreme value.	24
2.26	Comparison of all the j-V characteristics.	25
2.27	Comparison of all the j-P characteristics.	25
2.28	Thermal maps for $T \approx 45$ °C.	26
3.1	Comparison of $P_{loss}(D)$ characteristics of the 1st (disregarded) and 2nd 40 °C measurements without humidification.	29
3.2	Comparison of all the j-V characteristics, including the disregarded ones.	30
3.3	Comparison of all the j-P characteristics, including the disregarded ones.	30

List of Abbreviations

- PWM: Pulse-width modulation
- PEMFC: Polymer-electrolyte (or proton exchange) membrane fuel cell
- PEM: Polymer electrolyte membrane
- GDE: Gas diffusion electrode
- GDL: Gas diffusion layer
- MEA: Membrane electrode assembly
- j-V: The dependency of the voltage on current density
- j-P: The dependency of the power density on current density